Muchow, Marek; Polojärvi, Arttu

Discrete element simulations on pressure ridge formation : How the length-inclusion facilitates new research avenues

Published in:
Proceedings of the 27th IAHR International Symposium on Ice (Gdansk, 2024)

Published: 01/01/2024

Document Version
Publisher's PDF, also known as Version of record

Please cite the original version:
Muchow, M., & Polojärvi, A. (2024). Discrete element simulations on pressure ridge formation : How the length-inclusion facilitates new research avenues. In *Proceedings of the 27th IAHR International Symposium on Ice (Gdansk, 2024)* (IAHR International Symposium on Ice). International Association for Hydro-Environment Engineering and Research. https://www.iahr.org/library/infor?pid=30391

27th IAHR International Symposium on Ice

Gdańsk, Poland, 9 – 13 June 2024

Hosted by
Spain Water
and IWHR, China

Discrete element simulations on pressure ridge formation: How the length-inclusion facilitates new research avenues

Marek Muchow and Arttu Polojärvi

Aalto University, School of Engineering, Department of Mechanical Engineering,
P.O. Box 14100, FI-00076 Aalto, Finland
marek.muchow@aalto.fi, arttu.polojärvi@aalto.fi

Abstract: Discrete element method (DEM) simulations are an effective tool to investigate sea-ice ridge formation processes. While past DEM studies were two-dimensional and, thus, focused on cross-section of ridges, we present three-dimensional simulations of pressure ridge formation. These simulations include ridges of various lengths, to highlight how it affects the ice failure and ridging forces. Additionally, we demonstrate that half of the ice rubble within a ridge starts to move again after initial rest. This short case study highlights the potential of three-dimensional DEM simulations to contribute to knowledge about ice ridge characteristics.

Keywords: ice ridge, modelling, discrete element method

1. Introduction

Sea-ice pressure ridges form when ice floes, driven by winds and ocean currents, collide or a large ice floe is compressed and fails. While the ice converges, it breaks into ice rubble building a keel under water and a sail on top of the ice (Figure 1). Thus, ridging influences the local ice thickness and facilitates an increase in overall ice volume (e.g., von Albedyll, 2022). Consequently, ridges are also obstacles for winter navigation, being a main cause for accidents during winter navigation as shown by Banda et al. (2015) for the Finnish sea areas, and for planning of offshore wind turbines.

To understand ridge formation on engineering scale, researchers either dissect ridges in the field or use numerical simulations. Ridge dissection offers insight, for example, into ridge geometry, ice rubble distribution, ridge macro-porosities and material properties of ice (e.g., Leppäranta and Hakala, 1992; Høyland, 2007; Shafrova and Høyland, 2008). Past numerical simulations have been two-dimensional discrete element method (DEM) simulations describing a cross-section of a ridge with a focus on ridging forces (Hopkins, 1994, 1998; Hopkins et al., 1999; Damsgaard et al., 2021). The first three-dimensional DEM simulations of ridges are presented by Muchow and Polojärvi (2024) with these including the length of the ridge as well (Figure 1). Additionally, the detailed knowledge of ridging on engineering scale is needed to further develop sea-ice modelling. There is a need for operational sea-ice forecast models with an accurate representation of ridges and, on the other hand, for a better understanding of how to implement ridging into continuum models (Lipscomb et al. (2007)).
Here, we present a companion study to Muchow and Polojärvi (2024) that highlights the advantages of three-dimensional DEM simulations to understand various ice deformation processes during ice ridge formation. The inclusion of the length facilitates non-simultaneous failure, which reduces the amplitude of oscillations in the ridging force records. Additionally, we present a case study on the trajectories of the particles within the ice rubble of one ridge. We show that about half of the particles get reactivated after they came to rest when more ice keeps on being added to the ridge.

The paper is structured as follows. The numerical model is briefly explained in Section 2 as well as the setup and simulations used. Section 3 presents the results and discussions, and Section 4 concludes the paper.

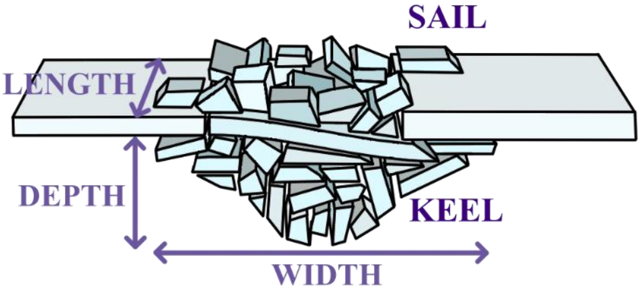

Figure 1: Schematic of a pressure ridge in three dimensions.

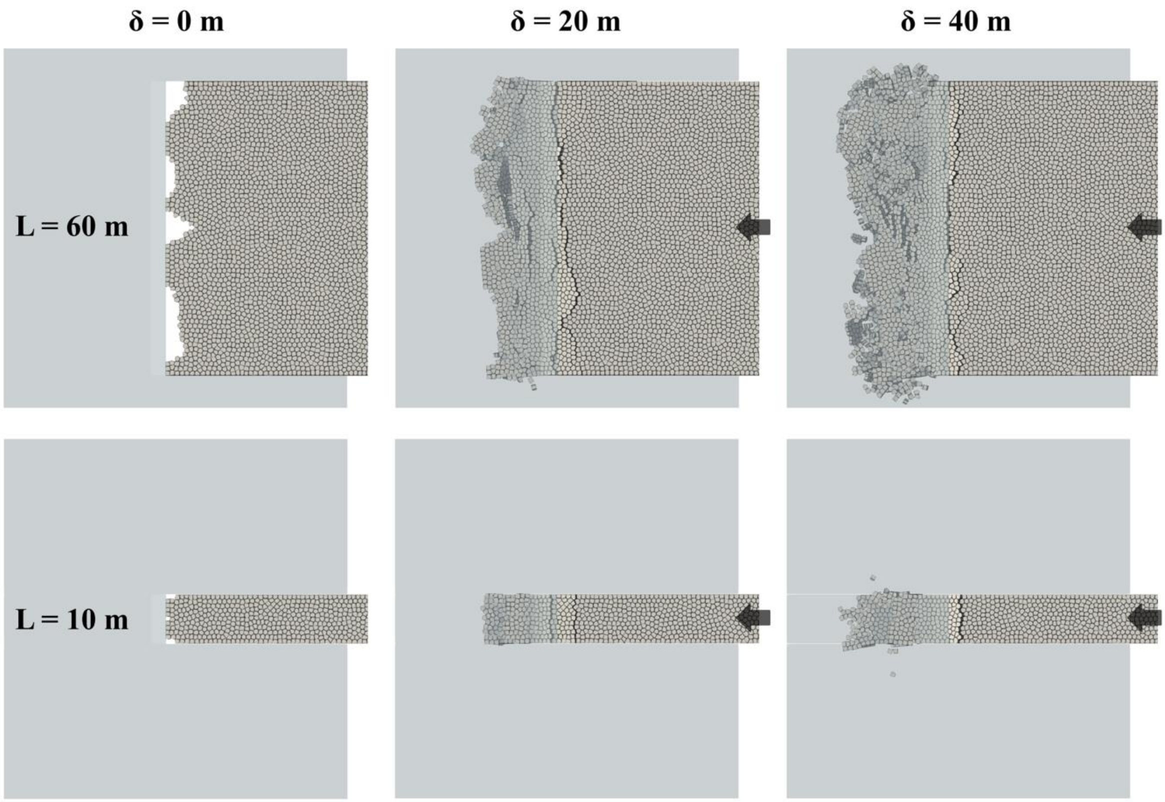

Figure 2: Snapshots of two ridging simulations with a different ridge length L at different stages of ice pushed δ into the ridge. The scale is constant across both simulations. The direction of ice velocity is indicated by the arrow.

2. Numerical model and setup

The numerical model describes ice-failure processes in three dimensions by utilizing the discrete element method (DEM). We employ the same setup as used in Muchow and Polojärvi (2024), which is validated against laboratory-scale ridging experiments. Additionally, the model was also successfully validated against laboratory-scale ice-structure interaction experiments by Polojärvi (2022). A detailed description of the model can be found in Polojärvi (2022). In brief, the model implementation follows that of a rather standard for DEM. In the model, the ice is described by rigid discrete particles, initially connected by finite beam elements, which deform and fail due to relative motion of the particle pair connected by each beam. The individual particles interact through pairwise contacts resulting in internal forces due to ice deformation and contact forces. Additional forces applied to each particle are external forces due to gravity, buoyancy and water drag.

During the ridge formation simulations, a deformable ice floe moves with a constant velocity v towards a thicker rigid floe (Figure 2). While the deformable floe fails against the rigid floe, followed by the formation of the ridge, we measure the ridging forces F at the rigid floe. The deformable floe features an uneven edge, while the edge of the rigid floe has a downward slope with an angle of about 30° to avoid high force peaks during initial contact and initialize riding. Additional ice on each side of the deformable floe restricts the ice from lateral movement. The rigid floe had a thickness about double of that of the ice used. The simulations parameters are presented and summarized in Table 1.

Table 1: Main simulation parameters, described in more detail Polojärvi (2022). The ice parameters are for the deformable floe.

Description		Value	Unit
General	Time step	$6 \cdot 10^{-6}$	s
	Gravitational acceleration	9.81	m/s^2
Ice	Thickness h	0.95	m
	Floe Width	60 … 10	m
	Floe Length	100 … 130	m
	Velocity	0.16	m/s
	Density	920	kg/m^3
Beams	Damping ratio	0.75	
	Elastic Modulus	270	MPa
	Tensile strength	100	kPa
	Shear strength	100	kPa
	Poisson's ratio	0.3	
	Mean length	h	m
Contact	Plastic limit	40	kPa
	Ice-ice friction	0.6	
Water	Density	1010	kg/m^3
	Drag coefficient	1.0	

With this setup, we investigated the influence of the ridge length L on F. L varied between 60 m, 30 m, and 10 m. For the 30 m and 10 m simulations we conducted two simulations each, while there are three simulations for the 60 m simulations. The 60 m simulations are also part of the analysis in Muchow and Polojärvi (2024). Each of the simulations featured differences in the particle shape and initial position as well as the edges of the deformable sheet, which results in different failure processes Polojärvi (2022).

3. Results and discussion

To investigate the advantages of three-dimensional DEM simulations over two-dimensional DEM simulations we compare simulations with different ridge lengths L ranging from 60 m, 30 m and 10 m with each other. Figure 2 compares simulation snapshots of a 60-meter-long ridge with a 10-meter-long ridge at instants of δ = 10, 20 and 40 m pushed into the ridge. The snapshots of the longer ridge show the approaching ice failing at different distances from the edge of the rigid floe in a manner resembling a non-simultaneous failure process (Sanderson 1988). Contrary to this behavior, the ice building the short ridge fails across the whole length of the ice floe in a virtually straight line. This failure process is comparable to two-dimensional simulations as most two-dimensional ridging simulations neglect the length of the ridge and only simulate ridging across one cross-section of the ridge (Hopkins, 1994 and 1998; Damsgaard et al., 2021). Additionally, the failure of the approaching floe does influence the shape of the ice rubble pile within the ridge. The rubble pile within the shorter ridge contains rubble pieces spanning across the whole length of the ridge after δ= 20 m. Simultaneously, the ice rubble within the larger ridge shows overall greater fragmentation. The visual comparison highlights how the length of the simulated ridge influences how the approaching ice fails and feeds into the ridge.

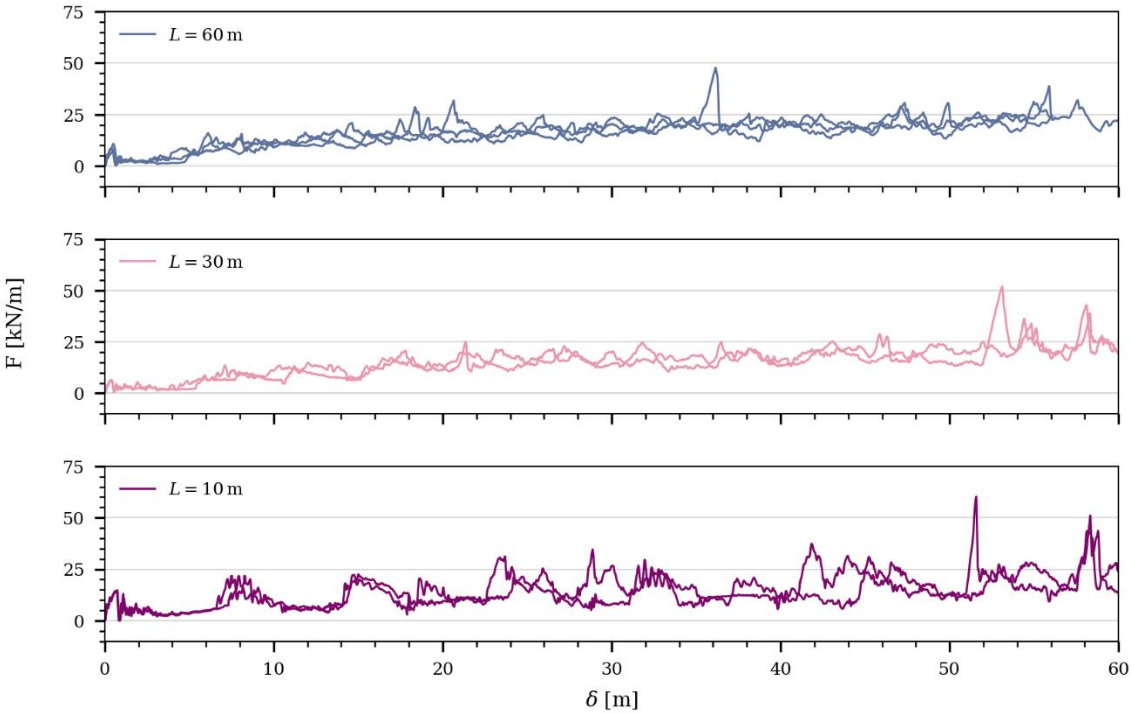

Figure 3: For different ridging simulations the ridging force F is displayed against the ice pushed δ into each ridge. F is normalized by the ridge length L, which decreases from top to bottom from 60 m to 30 m and 10 m.

Most DEM ridging simulations are conducted with the goal to understand ridging processes and how these relate to ridging forces. Figure 3 shows the record of the ridging forces F against the ice pushed δ into each ridge. To account for the different L, the F-δ records are normalized by L. With a decrease in L, the oscillations in the F-δ record increase. Additionally, the pattern of the F-δ record changes from $L = 30$ m to $L = 10$ m with 10-m-long ridge simulations showing periods of force buildup and failure ($\delta = 6$-10 m) followed by a nearly vanishing F ($\delta = 10$-12 m). This low value of F is due to the approaching ice losing contact with the rigid floe after failure at the floe edge. Contrary, for the longer ridges the approaching ice always remains in contact with the ice rubble or rigid floe. This contact is maintained due to non-simultaneous failure of the ice sheet resulting in an uneven edge creating partial contact (Figure 2). This effect on the ridging force can be further illustrated by a comparison of the standard deviation of the force recording calculated from $\delta = 30$-60 m, which increased by 90% from the 60-meter-long ridge to the 10-meter-long ridge. To summarize, including the length of the ridge into the ridging simulation allows for non-simultaneous failure to occur, which is integral for the ice failure and ridging forces and highlights the importance of three-dimensional simulations.

Further, we present a case study on ice rubble motion within the ridge to emphasize the potential of three-dimensional ridging simulations. To investigate how many particles get rearranged within the ridge, we isolated the trajectories of 1200 particles located within the first 20 m of the deformable floe for one of the 60-meter-long ridge simulations. To analyze the behavior of the particles within the ridge, we first defined that a particle came to rest, when its speed $v_p \leq 0.001$ m/s, which is a small fraction of the velocity of the deformable floe ($v_i = 0.16$ m/s). From the moment of rest onwards, we followed the motion of the particle and observed its displacement against δ, which draws the trajectory. Out of the initial 1200

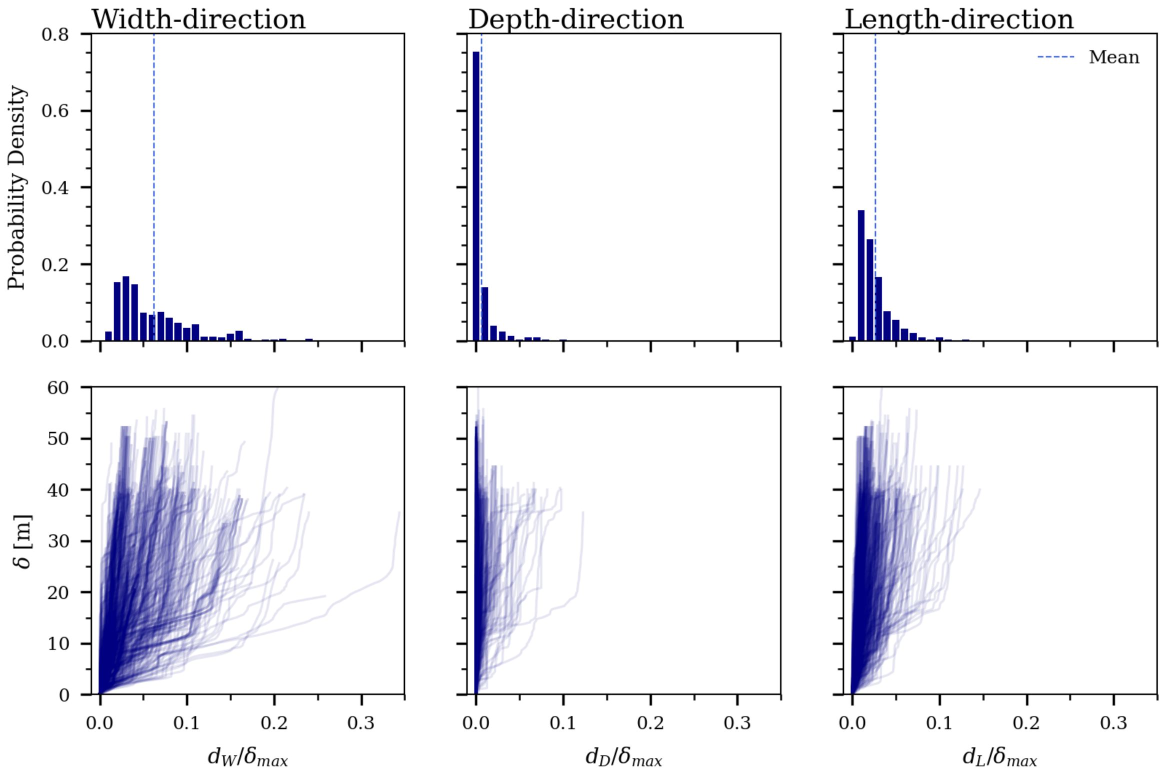

Figure 4: The total displacement d of 642 particles after rest is displayed in width-, depth- and length-direction as given in Figure 1. d is normalized by the total amount of ice pushed after rest, δ_{max}, to account for the different lengths of each particle trajectory. The top row shows the distribution of d/δ_{max} at the end of the simulation, while the bottom row shows the trajectory of each particle against the ice pushed after rest δ. The bin width of the histogram is 0.01.

particles, about 50 % started to move again after rest as well as having long enough ($\delta \geq 10$ m) trajectories to be included in the further analysis.

Figure 4 shows how the total displacement d, normalized by the total amount of ice pushed after rest δ_{max} is distributed across the particles, as well as trajectories of all particles with $\delta \geq 10$ m. We analyzed the displacement in width-, depth- and length-direction of the ridge (W, D and L as shown in Figure 1). The normalized particle displacements in the width-direction, d_W/δ_{max}, have the highest values, which would be expected, as the deformable floe moves into this direction. On the other hand, the particles hardly relocate in depth-direction, as manifested by nearly 80% of the particles being contained in the first bin of the histogram, meaning that they moved less than half a millimeter per meter of ice pushed. Movement of particles along length-direction is only possible in three-dimensional simulations. The average of the normalized displacement in this direction, d_L/δ_{max}, is about half of the average of d_W/δ_{max}. Additionally, the displacement in length-direction does not only occur in the particles on the outside edge of the ridge, as one might expect, but within the ridge as well. While the order of d_W/δ_{max} and d_L/δ_{max} is in centimeters per one meter of pushed ice, the result suggests the rubble distributes in both directions, a result which would not be captured by two-dimensional simulations.

Looking at the individual trajectories of particles after rest (Figure 4, bottom), it is also evident that the particles can go through several cycles of rest and reactivation. One example for this behavior in width-direction is a group of particles which stopped moving significantly from around $\delta = 10$ m to nearly $\delta = 20$ m. At $\delta = 20$ m this group experienced a significant displacement again.

As the model does not include thermodynamics, the ice rubble cannot build freeze-bonds. Since this study focuses only on an initial ridge formation, the absence of freeze-bonds likely does not affect the result. Additionally, we argue that the rearranging of the ice rubble could inhibit the freeze-bond formation. Further investigating the rubble in three-dimensional simulations could also add to knowledge gained from fieldwork about ridge characteristics. One example therefore is the macro-porosity in ridges, Currently, our simulation setup does not include splitting of particles, but the latter could be implemented based on Prasanna and Polojärvi 2023.

4. Summary and conclusions

This paper used a previously validated three-dimensional discrete element method (DEM) model to simulate development of pressure ridges (Muchow and Polojärvi, 2024). The results of this study are two-fold. First, we compare simulations with a varying ridge length with each other with a focus on ridging forces. Then we investigate how ice rubble within the ridge gets relocated as a case study. Both results highlight the importance of three-dimensional DEM simulations for a more accurate understanding of ridges.

Acknowledgments

The authors wish to acknowledge funding from the European Union –Next Generation EU instrument through the Academy of Finland under grant number (348586) WindySea – Modelling engine to design, assess environmental impacts, and operate wind farms for ice-covered waters. MM acknowledges funding from the AaltoENG 4-year doctoral program.

References

Banda, O.A.V., Goerlandt, F., Montewka, J. and Kujala, P., 2015. A risk analysis of winter navigation in Finnish sea areas. *Accident Analysis & Prevention*, *79*, pp.100-116.

Damsgaard, A., Sergienko, O. and Adcroft, A., 2021. The Effects of Ice Floe-Floe Interactions on Pressure Ridging in Sea Ice. *Journal of Advances in Modeling Earth Systems*, *13*(7), p.e2020MS002336.

Hopkins, M.A., Hibler III, W.D. and Flato, G.M., 1991. On the numerical simulation of the sea ice ridging process. *Journal of Geophysical Research: Oceans*, *96*(C3), pp.4809-4820.

Hopkins, M.A., 1994. On the ridging of intact lead ice. *Journal of Geophysical Research: Oceans*, *99*(C8), pp.16351-16360.

Hopkins, M.A., 1998. Four stages of pressure ridging. *Journal of Geophysical Research: Oceans*, *103*(C10), pp.21883-21891.

Høyland, K.V., 2007. Morphology and small-scale strength of ridges in the North-western Barents Sea. *Cold Regions Science and Technology*, *48*(3), pp.169-187.

Leppäranta, M. and Hakala, R., 1992. The structure and strength of first-year ice ridges in the Baltic Sea. *Cold Regions Science and Technology*, *20*(3), pp.295-311.

Lipscomb, W.H., Hunke, E.C., Maslowski, W. and Jakacki, J., 2007. Ridging, strength, and stability in high-resolution sea ice models. *Journal of Geophysical Research: Oceans*, *112*(C3).

Muchow, M and Polojärvi, A., 2024, Three-dimensional discrete element simulations on pressure ridge formation. *EGUsphere [preprint], https://doi.org/10.5194/egusphere-2024-831*
Polojärvi, A., 2022. Numerical model for a failure process of an ice sheet. *Computers & Structures*, *269*, p.106828.
Prasanna, M. and Polojärvi, A., 2023. Breakage in quasi-static discrete element simulations of ice rubble. *International Journal of Mechanical Sciences*, *259*, p.108595.
Sanderson, T.J., 1988. Ice mechanics and risks to offshore structures.
Shafrova, S. and Høyland, K.V., 2008. Morphology and 2D spatial strength distribution in two Arctic first-year sea ice ridges. *Cold Regions Science and Technology*, *51*(1), pp.38-55.
von Albedyll, L., Hendricks, S., Grodofzig, R., Krumpen, T., Arndt, S., Belter, H.J., Birnbaum, G., Cheng, B., Hoppmann, M., Hutchings, J. and Itkin, P., 2022. Thermodynamic and dynamic contributions to seasonal Arctic sea ice thickness distributions from airborne observations. *Elem Sci Anth*, *10*(1), p.00074.